6
Implications of nuclear symmetry energy on NS matter equation of state

6.1 Introduction

As previously mentioned, the interior of NS is a good domain to study dense nuclear matter in bulk with and without exotic degrees of freedom. In general, we have good knowledge about finite nuclei at saturation density. Hence, the theoretical idea of uniform symmetric nuclear matter in bulk even at large densities above n_0 is just the extrapolation and idealization of finite nuclei knowledge. One important ingredient for the calculation of the energy density of nucleons inside nuclear matter is the symmetry energy ($E_{\rm sym}$). Consequently, nuclear symmetry energy and its density dependence play a significant role in comprehending dense matter behaviour [Ducoin et al., 2010; Lattimer and Prakash, 2016]. In case of finite nuclei, the contribution of symmetry energy to the mass of nuclei is small compared to other terms in the semi-empirical mass formula [Kirson, 2008]. The nuclear symmetry energy and its variation with density affects substantially the composition and matter pressure what in consequence affects the NS properties specially the radius [Centelles et al., 2009; Fattoyev et al., 2018]. GW observations set bound on the mutual tidal deformability ($\tilde{\Lambda}$) which also depends on matter properties linked to $E_{\rm sym}$. A comprehensive idea regarding symmetry energy behaviour can be gathered via studying its effects on other NS properties such as maximum mass, compactness and tidal deformability.

Many recent studies have been done to constrain the values of $E_{\rm sym}$ at n_0 and its slope ($L_{\rm sym}$) at n_0 based on data from various astrophysical observations as well as terrestrial experiments [Lattimer and Steiner, 2014a; Roca-Maza et al., 2015; Tews et al., 2017]. Very recently an improved value of neutron skin thickness of ^{208}Pb was reported in Lead Radius EXperiment-II (PREX-2) to be $R_{\rm skin} = R_n - R_p = (0.283 \pm 0.071)$ fm [Adhikari et al., 2021]. This evaluates the corresponding symmetry energy and its slope to be $E_{\rm sym} = (38.1 \pm 4.7)$ MeV and $L_{\rm sym} = (106 \pm 37)$ MeV respectively at n_0 with correlation coefficient as 0.978 [Reed et al., 2021]. These updated values of isospin asymmetry parameters are larger than the ones (28.5 MeV $\leq E_{\rm sym}(n_0) \leq$ 34.9 MeV; 30.6 MeV $\leq L_{\rm sym}(n_0) \leq$ 86.8 MeV) previously reported in ref.-Oertel et al. [2017] obtained by comparison of experimental data from finite nuclei and heavy-ion collisions with different microscopic model calculations. Another nuclear saturation parameter, the curvature of symmetry energy $K_{\rm sym}$ has been studied in recent years with predicted range values -111.8 ± 71.3 MeV [Mondal et al., 2017], -85^{+82}_{-70} MeV [Baillot d'Etivaux et al., 2019], -102^{+71}_{-72} MeV Zimmerman et al. [2020] at n_0 based on nuclear and

astrophysical observational data which put additional constraint on dense matter EoS.

In this chapter, we explore the influence of nuclear symmetry energy on dense matter EoS, consequently on NS properties. To do so, we consider RMF model implementing the density-dependence of isovector-vector coupling as introduced in ref.-Spinella [2017] and incorporating non-linear GM1 [Glendenning and Moszkowski, 1991] and density dependent DD-MEX [Taninah et al., 2020] coupling parametrizations. In the RMF scheme, the coupling constants are chosen in such a way that the model can reproduce the experimental quantities known at n_0. Thus the observational properties of NSs which depend on the EoS parameters *i.e.* coupling constants, will determine $E_{\rm sym}$ and $L_{\rm sym}$. In several previous studies the symmetry energy effects on dense matter has been considered with the matter composition to be purely nucleonic [Ji et al., 2019; Hu et al., 2020; Wu et al., 2021]. This work is dedicated to explore the novel aspects of density-dependent isovector coupling on dense matter EoS with the onset of heavier strange and non-strange degrees of freedom and study the symmetry energy slope effects on NS properties.

This chapter is based on the work Thapa and Sinha [2022] and is organized as follows. In sec.-6.2, a brief introduction on nuclear symmetry energy is provided. This is followed by describing the formalism and coupling parameter sets implemented in this work in sec.-6.3, 6.4. The effects of nuclear symmetry energy on dense matter are shown and discussed in sec.-6.5. Finally, the summary and concluding remark of this work are provided in sec.-6.6.

6.2 Nuclear symmetry energy

The isospin dependence of asymmetric dense nuclear matter is represented by the nuclear symmetry energy and it has a vital role to play in studying neutron rich nuclei. $E_{\rm sym}$ and its density dependence are important to get the idea about the isovector-vector meson coupling constants g_ρ and its variation with density. In terms of energy density we can get the values of $E_{\rm sym}$ by the Taylor's expansion of the energy density of symmetric nuclear matter (NM) in terms of neutron-proton asymmetry factor, $\alpha = (n_n - n_p)/n$

$$\varepsilon(n,\alpha) = \varepsilon(n,0) + \frac{1}{2}\left[\frac{\partial^2\varepsilon(n,\alpha)}{\partial\alpha^2}\right]_{\alpha=0}\alpha^2 + \mathcal{O}(\alpha^4), \tag{6.1}$$

where n, n_n, n_p denote the baryon number, vector number densities of neutron and proton respectively. $\varepsilon(n,0)$ is the energy density of symmetric nuclear matter. The coefficient of second term in eq.-(6.1) refers to the nuclear symmetry energy $E_{\rm sym}(n)$. Subsequent expansion of $E_{\rm sym}(n)$ around n_0 provides Matsui [1981]; Chen and Piekarewicz [2014]

$$E_{\rm sym}(n) = E_{\rm sym}(n_0) + L_{\rm sym}(n_0)\zeta + \frac{1}{2}K_{\rm sym}(n_0)\zeta^2 + \mathcal{O}(\zeta^3), \tag{6.2}$$

where $\zeta = (n - n_0)/3n_0$, $E_{\rm sym}(n_0)$ denotes the nuclear symmetry energy at nuclear saturation density. The slope and curvature of symmetry energy coefficient at n_0 are represented respectively by

$$L_{\rm sym}(n_0) = 3n_0\left[\frac{\partial E_{\rm sym}(n)}{\partial n}\right]_{n=n_0}, \quad K_{\rm sym}(n_0) = 9n_0^2\left[\frac{\partial^2 E_{\rm sym}(n)}{\partial n^2}\right]_{n=n_0}. \tag{6.3}$$

Table 6.1: a_ρ coefficient values for various estimations of $L_{\rm sym}(n_0)$ and corresponding $K_{\rm sym}(n_0)$ for GM1 and DD-MEX coupling models.

$L_{\rm sym}(n_0)$ (MeV)	a_ρ		$K_{\rm sym}(n_0)$ (MeV)	
	GM1	DD-MEX	GM1	DD-MEX
35	0.5893	0.8052	−127.13	−34.44
50	0.4390	0.6148	−129.67	−72.21
65	0.2888	0.4242	−105.17	−75.72
85	0.0885	0.1702	−30.43	−27.06

6.3 Formalism

The theoretical framework to construct the dense matter EoS for baryon octet as well as Δ-resonances is already described in sec.-4.2. The interaction between non-strange baryons are described via the exchange of isoscalar-scalar σ, isoscalar-vector ω, and isovector-vector ρ mesons. For the hyperonic sector interactions, an additional hidden strangeness isoscalar-vector ϕ meson is taken into consideration to describe the hyperon-hyperon repulsive interactions. In this study too, we have not considered the contribution from scalar hidden strangeness σ^*-meson due to the reason already mentioned in sec.-5.2.

6.4 Coupling parameters

As mentioned earlier in sec.-6.1, in the present work, we implement GM1 and DD-MEX parametrizations. In case of GM1 parametrization, the density dependent coupling constant for the isovector ρ-meson is given by

$$g_{\rho N}(n) = g_{\rho N}(n_0) e^{-a_\rho (x-1)}, \tag{6.4}$$

where $x = n/n_0$, while the coupling constants for σ, ω-mesons are considered to be density-independent. Table-2.3 provides the parameter values of GM1 and DD-MEX coupling parametrizations in nucleonic sector. In the standard GM1 parametrization, $g_{\rho N}$ is density independent and for the standard DD-MEX parametrization the coefficient a_ρ is given in table-2.3. For variation in $L_{\rm sym}$, it is evaluated by calibrating the coefficient a_ρ without altering the other nuclear saturation properties. Since the non-strange baryons do not couple with ϕ-meson, $g_{\phi N} = g_{\phi \Delta} = 0$.

The values of coefficient a_ρ adjusted to estimate different values of $L_{\rm sym}$ at n_0 for GM1 and DD-MEX parametrizations are provided in table-6.1.

For the hyperonic sector, the vector couplings are implemented according to SU(6) symmetry and quark counting rule [Schaffner et al., 1994]. And for the scalar couplings, we consider the optical potential values in symmetric nuclear matter as [Gomes et al., 2015; Gal et al., 2016]

$$U_\Lambda^{(N)}(n_0) = -30 \text{ MeV}, \quad U_\Xi^{(N)}(n_0) = -14 \text{ MeV}, \quad U_\Sigma^{(N)}(n_0) = +30 \text{ MeV}. \tag{6.5}$$

Table-6.2 provides the scalar meson-hyperon coupling values at n_0.

Table 6.2: Scalar meson-hyperon coupling constants, $R_{\sigma Y} = g_{\sigma Y}/g_{\sigma N}$ (normalized to meson-nucleon coupling) for considered parametrizations in this work.

	Λ	Σ	Ξ
GM1	0.6164	0.4033	0.3047
DD-MEX	0.6172	0.4734	0.3088

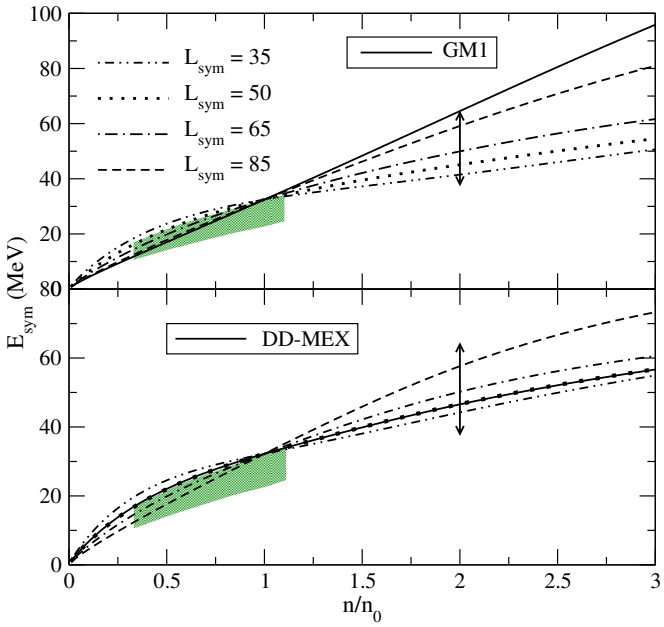

Figure 6.1: Nuclear symmetry energy as a function of baryon number density (in units of n_0) for, upper panel: GM1 and lower panel: DD-MEX coupling parametrizations. The shaded regions denote the constraints on density-dependent symmetry energy from heavy-ion collision data [Tsang et al., 2009, 2011]. The constraint $38 \leqslant E_{\rm sym}(2n_0)/{\rm MeV} \leqslant 64$ Li et al. [2021a] at 68% confidence level obtained via analyses of data from recent NS observables and heavy-ion collisions is denoted by the vertical error bars. The solid lines in both the panels represent the original coupling parametrizations. The other cases with adjusted values of $L_{\rm sym}$ at n_0 are denoted by dot-dot-dashed ($L_{\rm sym} = 35$), dotted ($L_{\rm sym} = 50$), dash-dotted ($L_{\rm sym} = 65$) and dashed ($L_{\rm sym} = 85$) curves respectively.

And for the Δ-resonance sector, we consider $R_{\omega\Delta} = 1.10$ and $R_{\rho\Delta} = 1.00$ in the vector coupling sector. And in the scalar meson-Δ resonance coupling sector, we consider two cases of $R_{\sigma\Delta} = 1.10, 1.20$.

6.5 Results and discussion

In this section, we report the numerical results for purely nucleonic (N), hypernuclear (NY) and Δ-admixed hypernuclear (NYΔ) matter compositions and investigate the effects of symmetry energy on dense matter EoS. In order to do so, as mentioned in sec.-6.1, we implement the density-dependent modification in isovector $g_{\rho b}$ couplings within the frame-

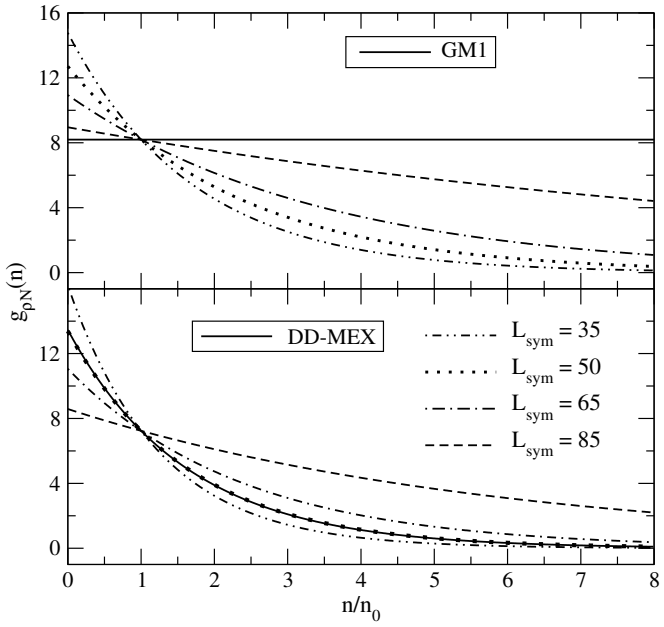

Figure 6.2: Isovector coupling to nucleons as a function of baryon number density (in units of n_0) in case of GM1 (upper panel) and DD-MEX (lower panel) parametrizations. The different curves represent the same cases as captioned in fig.-6.1.

works of non-linear (GM1) and consider the density-dependent coupling schemes with DD-MEX parametrizations. We proceed by studying the effect of variation of $L_{\rm sym}$ on different properties of matter and stars.

The behaviour of nuclear symmetry energy with varying baryon number density is plotted in fig.-6.1 for different values of $L_{\rm sym}$. In density regime $n < n_0$, cases with higher values of $L_{\rm sym}$ yield lower values of $E_{\rm sym}$ while the vice-versa is observed in case of higher density regimes ($n > n_0$). From the relation E/A(pure neutron matter) $\approx E/A$(symmetric nuclear matter) + $E_{\rm sym}$, where E/A denote the energy per nucleon, it can understood that the $L_{\rm sym}$ dependence of E/A is very similar to that $E_{\rm sym}$. Due to the isovector meson-nucleon coupling's relation given by eqn.-(6.4), the $E_{\rm sym}$ values are observed to be lower (higher) with different $L_{\rm sym}$ for $n < n_0$ ($n > n_0$) to evaluate the same $E_{\rm sym}$ value at n_0. The experimental constraints on $E_{\rm sym}(n)$ at sub-saturation densities shown by the shaded region in the fig.-6.1 allow EoSs with $L_{\rm sym}(n_0) \geqslant 50$ MeV. The values of $E_{\rm sym}$ at n_0 are same for all values of $L_{\rm sym}$ as it is constrained by the isovector coupling value at nuclear saturation. This result is consistent with that of ref.-Wu et al. [2021] found considering NL3 [Lalazissis et al., 1997] parametrization. The constraint on $E_{\rm sym}(2n_0)$ is broader and allows for almost all EoSs corresponding to $L_{\rm sym}(n_0)$ values considered in this work.

Fig.-6.2 displays the density-dependent nature of isovector couplings in variation with baryon number density for different values of $L_{\rm sym}$ in both coupling schemes. In sub-saturation densities, it is observed that with lower $L_{\rm sym}$ values, the isovector coupling values are larger. This behaviour is vice-versa in supra-saturation density regimes. At the saturation density, $g_{\rho N}$ values are identical owing to eq.-(6.4). With higher values of $L_{\rm sym}$, the variation of $g_{\rho N}$ with baryon number density is found to be more steep. The $g_{\rho N}(n)$ coupling values with lower $L_{\rm sym}$ approach zero at high density regimes resulting in similar corresponding $E_{\rm sym}(n)$ values

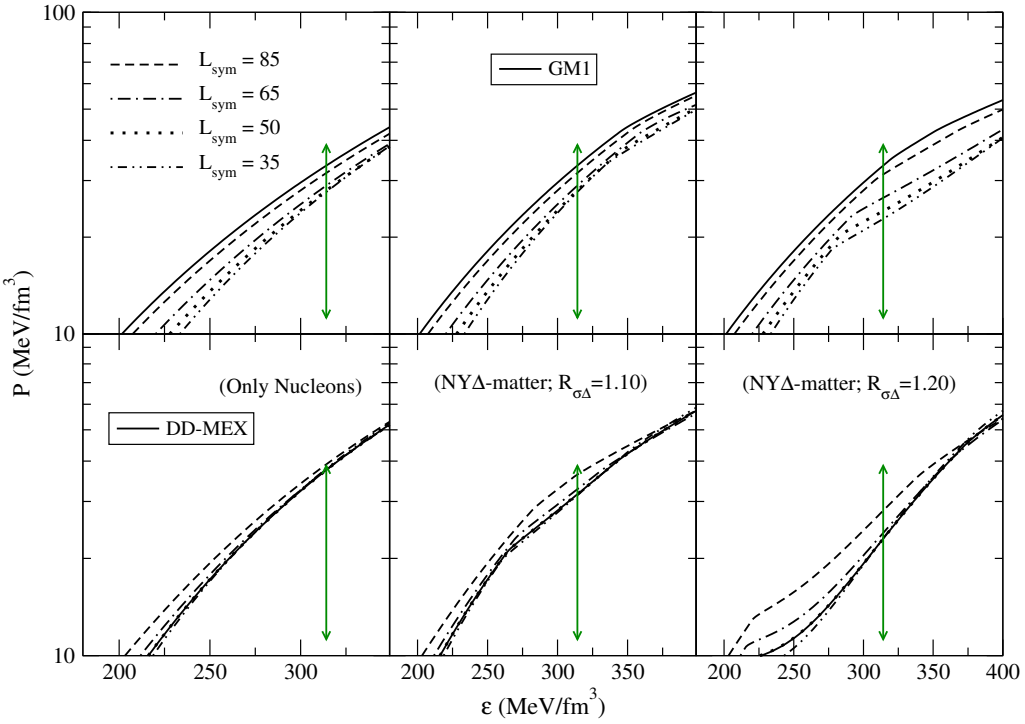

Figure 6.3: Pressure variation as a function of energy density (EOS) for $T = 0$ case with matter compositions as, left panels: pure nucleonic, middle panels: NYΔ ($R_{\sigma\Delta} = 1.10$) and right panels: NYΔ ($R_{\sigma\Delta} = 1.20$) for different $L_{\rm sym}(n_0)$ values in upper panels: GM1 and lower panels: DD-MEX parametrizations. The different curves represent the same cases as captioned in fig.-6.1. The matter pressure constraint (vertical line) at $n \sim 2n_0$ is deduced from GW170817 [Abbott et al., 2018] event data.

at those densities.

The EoSs for different NS matter compositions (N, NYΔ) are presented in fig.-6.3 for GM1 parametrization in upper panels and for DD-MEX parametrization in lower panels. The EoSs with modified isovector couplings within non-linear GM1 model as well as with DD-MEX parametrization are observed to lie well within bounds of the matter pressure constraint from GW170817 event data [Abbott et al., 2018] shown by the vertical arrows in fig.-6.3. This is true for all the matter composition cases. The prominent differences in EoSs are observed at low density regimes ($n \leqslant 0.4$ fm^{-3}).

Tables-6.3 and 6.4 provide the threshold densities of heavier baryons in NY and NYΔ matter with GM1 and DD-MEX coupling parametrizations respectively. It is observed that low values of $L_{\rm sym}$ shifts the onset of hyperons to higher density regimes. While the opposite behaviour is seen in case of Δ-resonances. Higher values of normalized scalar meson-Δ couplings denote attractive Δ-potentials in symmetric nuclear matter which result in early appearance of Δ-quartet in NS matter. Onset of Δ-resonances delay the appearance of hyperons in NS matter.

It is observed that onset of heavier baryons softens the EoSs marked by change in slopes as shown in fig.-6.3. Now at high matter densities, $g_{\rho b}(n)$ coupling values tend to approach zero resulting in less contribution to EoSs from ρ-meson fields. With increase in attractive

Table 6.3: Threshold densities, n_u for hyperons and Δ-quartet in NY and NYΔ matter with varying $L_{\rm sym}$ at n_0 values in GM1 parametrization.

Model	$R_{\sigma\Delta}=0$	$R_{\sigma\Delta}=1.10$		$R_{\sigma\Delta}=1.20$	
	$n_u^Y\ (n_0)$	$n_u^Y\ (n_0)$	$n_u^\Delta\ (n_0)$	$n_u^Y\ (n_0)$	$n_u^\Delta\ (n_0)$
GM1	2.25	2.25	2.89	2.29	2.11
$L_{\rm sym}=35$	2.54	2.68	2.22	2.95	1.87
$L_{\rm sym}=50$	2.49	2.57	2.27	2.84	1.90
$L_{\rm sym}=65$	2.42	2.43	2.35	2.66	1.94
$L_{\rm sym}=85$	2.30	2.30	2.61	2.39	2.04

Table 6.4: Similar to table-6.3 but with DD-MEX parametrization.

Model	$R_{\sigma\Delta}=0$	$R_{\sigma\Delta}=1.10$		$R_{\sigma\Delta}=1.20$	
	$n_u^Y\ (n_0)$	$n_u^Y\ (n_0)$	$n_u^\Delta\ (n_0)$	$n_u^Y\ (n_0)$	$n_u^\Delta\ (n_0)$
DD-MEX	2.13	2.27	1.79	2.47	1.46
$L_{\rm sym}=35$	2.15	2.31	1.77	2.51	1.44
$L_{\rm sym}=50$	2.13	2.27	1.79	2.47	1.46
$L_{\rm sym}=65$	2.09	2.19	1.82	2.39	1.47
$L_{\rm sym}=85$	2.03	2.07	1.89	2.24	1.50

Δ-potential, the onset of Δ^- shifts towards lower density regimes as marked by the kinks in fig.-6.3.

The mass-radius relationships obtained by solving TOV equations for non-rotating, spherically symmetric stars corresponding to the EOSs for N, NYΔ ($R_{\sigma\Delta}=1.10,\ 1.20$) matter with GM1 and DD-MEX parametrizations are displayed in different panels of fig.-6.4. For the crust region, Baym-Pethick-Sutherland (BPS) [Baym et al., 1971b] and Baym, Bethe, Pethick (BBP) [Baym et al., 1971a] EoSs are implemented maintaining thermodynamic consistency while modelling crust-core transition following ref.-Fortin et al. [2016]. It can be observed that almost all EoSs (in N, NYΔ-matter compositions) fit within the limits of recent astrophysical constraints. However, the joint constraints on radius of a 1.4 $M_\odot$ NS Jiang et al. [2020]; Landry et al. [2020] are satisfied by EoS models with $L_{\rm sym}\leq 65$ MeV. Incorporation of Δ-quartet further softens the EoS at lower density in addition to high density regimes leading to NS configurations with smaller radii as evident from middle and right panels of fig.-6.4. The nature of the secondary compact component involved in GW190814 as a NS is still not completely univocal [Sedrakian et al., 2020; Jie Li et al., 2020], hence the maximum mass constraint from this candidate is not stringent. The variation of symmetry energy slope has slight impact on maximum mass NS configurations owing to the similar values of $M_{\rm max}$ (refer to tables-6.5, 6.6). The softening of EoSs due to inclusion of Δ-resonances is more protruding in density-dependent scenario. The effect of varying $L_{\rm sym}$ is less for pure nucleonic matter and large for NYΔ-matter (with more attractive Δ-potential). For DD-MEX coupling parametrization, the maximum mass NS configuration with purely nucleonic matter reaches $\sim 2.55 M_\odot$ satisfying the mass constraint from GW190814 event. This is consistent with the results in ref.-Rather et al. [2021].

The particle abundances in NYΔ-matter composition ($R_{\sigma\Delta}=1.20$) with GM1 (with-

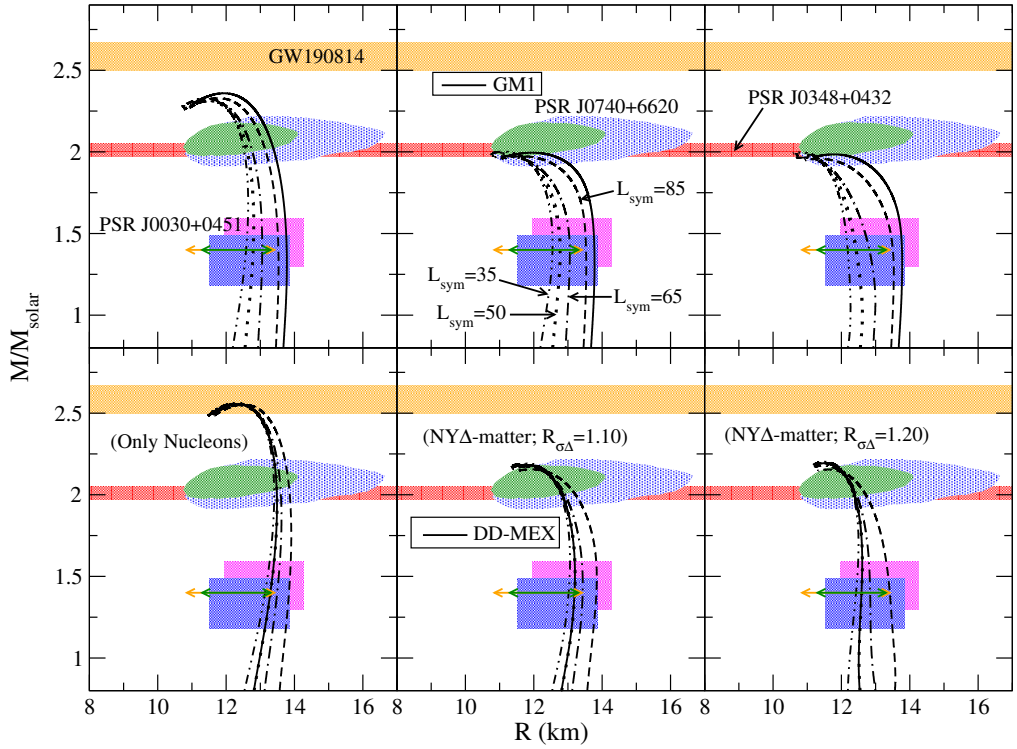

Figure 6.4: Solutions of TOV equations corresponding to left panels: pure N-matter, middle panels: NYΔ ($R_{\sigma\Delta} = 1.10$) and right panels: NYΔ ($R_{\sigma\Delta} = 1.20$) EoSs displayed in fig.-6.3 for upper panels: GM1 and lower panels: DD-MEX parametrizations. The different curves represent the same cases as captioned in fig.-6.1. The astrophysical observable constraints from GW190814 [Abbott et al., 2020b], PSR J0740 + 6620 [Riley et al., 2021; Miller et al., 2021], PSR J0348 + 0432 [Antoniadis et al., 2013] and PSR J0030 + 0451 [Miller et al., 2019; Riley et al., 2019] are represented by shaded regions. The horizontal lines represent the joint radius constraints from PSR J0030 + 0451 and GW170817 event data for a typical 1.4 $M_\odot$ NS [Jiang et al., 2020; Landry et al., 2020].

out density dependent $g_{\rho N}$) and with $L_{\rm sym}(n_0) = 50$ MeV coupling parametrization models are shown in fig.-6.5. It is observed that in case of density-dependent $g_{\rho N}(n)$ coupling (lower panel), the onset of hyperons is shifted to higher densities and early appearance of Δ-resonances is favoured. This resulted in faster decrease of lepton populations in comparison to constant $g_{\rho N}(n_0)$ coupling case (upper panel). In $g_{\rho N}(n_0)$ case, the Δ^-, Ξ^-, e^-, μ^- composition provides the negative charge to balance the proton charge resulting in appearance of Λ-hyperons. At high density regimes, this negative particle composition leads to onset of Δ^0 and Ξ^0 baryons. While in case of $g_{\rho N}(n)$ couplings, the onset of Δ^0 baryons are due to charge neutrality condition maintained by Δ^-, e^- with protons. Fig.-6.6 displays the particle populations as a function of baryon number density similar to fig.-6.5 but with DD-MEX parametrization for NYΔ-matter. It is also observed that with decrasing value of $L_{\rm sym}$, the onset of hyperons is shifted to higher densities while early onset of Δ-quartet is favoured. At sub-saturation densities, the charged particle abundances are enhanced with lower value of $L_{\rm sym}$. In case of $L_{\rm sym} = 49.57$ MeV (upper panel), the lepton populations are seen to decrease at a faster rate with rising matter density in comparison to $L_{\rm sym} = 85$ MeV (lower panel) case. This is because in the latter case Δ^- abundances fall short to maintain the charge neutrality condition with protons demanding lepton populations to stay till higher density regimes.

Table 6.5: NS properties evaluated from the EOS considering various matter compositions (N, NY, NYΔ) with varying $L_{\rm sym}(n_0)$ values with non-linear (GM1) and density-dependent (DD-MEX) coupling schemes. The maximum gravitational mass NS and its corresponding radius are denoted by $M_{\rm max}$ and R respectively; central number density, central energy density, central matter pressure are represented by n_c, ε_c and P_c. Matter pressures at 2 and 6 times saturation densities are denoted by $P(2n_0)$ and $P(6n_0)$ respectively. The global properties such as radius, compactness parameter, tidal Love number and tidal deformability for a $1.4M_\odot$ NS are given by $R_{1.4}$, $C_{1.4}$, $k_{2(1.4)}$ and $\Lambda_{1.4}$ respectively.

Matter composition	RMF Model		$M_{\rm max}$ ($M_\odot$)	R (km)	n_c (fm^{-3})	ε_c (MeV/fm^3)	P_c (MeV/fm^3)	$P(2n_0)$ (MeV/fm^3)	$P(6n_0)$ (MeV/fm^3)	$R_{1.4}$ (km)	$C_{1.4}$	$k_{2(1.4)}$	$\Lambda_{1.4}$
Pure Nucleonic Matter	NL	GM1	2.36	11.93	0.865	1116.75	500.67	30.48	574.12	13.77	0.150	0.100	882
		$L_{\rm sym}=85$	2.33	11.77	0.888	1145.36	512.52	28.62	553.83	13.53	0.153	0.098	785
		$L_{\rm sym}=65$	2.31	11.51	0.917	1185.47	547.87	25.54	549.66	13.06	0.158	0.096	640
		$L_{\rm sym}=50$	2.32	11.45	0.919	1186.87	555.04	24.22	554.15	12.79	0.162	0.096	581
		$L_{\rm sym}=35$	2.33	11.42	0.916	1180.98	553.01	23.59	556.13	12.58	0.164	0.102	568
	DD	DD-MEX	2.56	12.33	0.776	1000.40	487.24	32.26	704.96	13.29	0.156	0.106	773
		$L_{\rm sym}=85$	2.55	12.50	0.767	988.90	469.57	34.70	698.51	13.84	0.149	0.105	939
		$L_{\rm sym}=65$	2.55	12.36	0.777	1003.21	486.80	32.74	703.14	13.49	0.153	0.104	821
		$L_{\rm sym}=50$	2.56	12.33	0.776	1000.68	487.42	32.27	704.93	13.30	0.155	0.105	772
		$L_{\rm sym}=35$	2.56	12.31	0.773	995.26	484.09	32.31	705.36	13.14	0.157	0.108	748
Hypernuclear Matter	NL	GM1	1.99	11.97	0.926	1126.57	317.96	30.48	312.09	13.77	0.150	0.101	882
		$L_{\rm sym}=85$	1.98	11.72	0.964	1179.58	345.34	28.62	310.77	13.53	0.153	0.098	785
		$L_{\rm sym}=65$	1.98	11.41	1.001	1233.99	382.86	25.54	317.59	13.06	0.158	0.095	639
		$L_{\rm sym}=50$	2.00	11.37	0.994	1222.21	379.64	24.22	320.41	12.79	0.162	0.096	581
		$L_{\rm sym}=35$	2.01	11.36	0.983	1203.98	371.28	23.59	321.37	12.58	0.164	0.102	568
	DD	DD-MEX	2.18	12.00	0.875	1082.30	362.19	32.26	395.89	13.29	0.156	0.106	777
		$L_{\rm sym}=85$	2.16	12.14	0.876	1085.95	357.77	34.70	390.54	13.83	0.149	0.105	937
		$L_{\rm sym}=65$	2.17	12.02	0.882	1093.24	367.13	32.74	395.07	13.49	0.153	0.104	821
		$L_{\rm sym}=50$	2.18	12.00	0.876	1082.86	362.48	32.27	395.88	13.30	0.155	0.105	774
		$L_{\rm sym}=35$	2.19	11.99	0.869	1071.27	356.43	32.31	396.04	13.14	0.157	0.108	748

Table 6.6: Continuation of table-6.5.

Matter composition	RMF Model		$M_{\max}$ ($M_\odot$)	R (km)	n_c (fm^{-3})	ε_c (MeV/fm^3)	P_c (MeV/fm^3)	$P(2n_0)$ (MeV/fm^3)	$P(6n_0)$ (MeV/fm^3)	$R_{1.4}$ (km)	$C_{1.4}$	$k_{2(1.4)}$	$\Lambda_{1.4}$
Δ-admixed Hypernuclear Matter ($R_{\sigma\Delta} = 1.10$)	NL	GM1	1.99	11.95	0.928	1130.21	320.17	30.48	312.53	13.77	0.150	0.101	882
		$L_{\rm sym} = 85$	1.97	11.63	0.980	1204.54	360.38	28.62	312.22	11.63	0.153	0.098	785
		$L_{\rm sym} = 65$	1.97	11.19	1.045	1302.99	428.33	25.54	324.02	13.05	0.158	0.095	637
		$L_{\rm sym} = 50$	1.99	11.13	1.042	1297.38	429.21	24.22	328.62	12.77	0.162	0.095	570
		$L_{\rm sym} = 35$	2.00	11.11	1.031	1278.87	420.59	23.59	330.15	12.55	0.165	0.100	551
	DD	DD-MEX	2.18	11.75	0.911	1138.96	405.08	28.03	406.19	13.19	0.157	0.102	717
		$L_{\rm sym} = 85$	2.16	11.92	0.909	1138.40	395.67	33.15	398.31	13.83	0.149	0.104	935
		$L_{\rm sym} = 65$	2.17	11.76	0.918	1152.14	411.28	29.43	405.19	13.43	0.154	0.102	788
		$L_{\rm sym} = 50$	2.18	11.75	0.911	1139.52	405.38	28.06	406.18	13.20	0.157	0.102	720
		$L_{\rm sym} = 35$	2.19	11.74	0.904	1127.36	398.93	27.51	406.38	13.02	0.159	0.104	686
Δ-admixed Hypernuclear Matter ($R_{\sigma\Delta} = 1.20$)	NL	GM1	1.99	11.78	0.962	1179.86	345.22	30.48	313.94	13.77	0.150	0.101	881
		$L_{\rm sym} = 85$	1.96	11.34	1.037	1290.93	410.47	28.62	316.04	13.50	0.153	0.097	773
		$L_{\rm sym} = 65$	1.97	10.87	1.102	1392.46	488.48	24.65	332.45	12.82	0.161	0.089	541
		$L_{\rm sym} = 50$	1.98	10.82	1.094	1377.87	485.28	22.32	338.37	12.43	0.166	0.086	449
		$L_{\rm sym} = 35$	2.00	10.81	1.083	1358.24	476.19	20.88	340.33	12.18	0.169	0.083	395
	DD	DD-MEX	2.19	11.48	0.938	1177.66	439.80	18.67	416.19	12.59	0.164	0.090	505
		$L_{\rm sym} = 85$	2.15	11.62	0.945	1193.37	436.81	24.49	405.46	13.41	0.154	0.094	720
		$L_{\rm sym} = 65$	2.18	11.48	0.947	1194.49	447.69	20.08	414.88	12.84	0.161	0.089	565
		$L_{\rm sym} = 50$	2.19	11.48	0.938	1177.94	439.93	18.69	416.17	12.59	0.164	0.090	506
		$L_{\rm sym} = 35$	2.20	11.47	0.930	1165.22	433.33	18.30	416.43	12.43	0.166	0.093	487

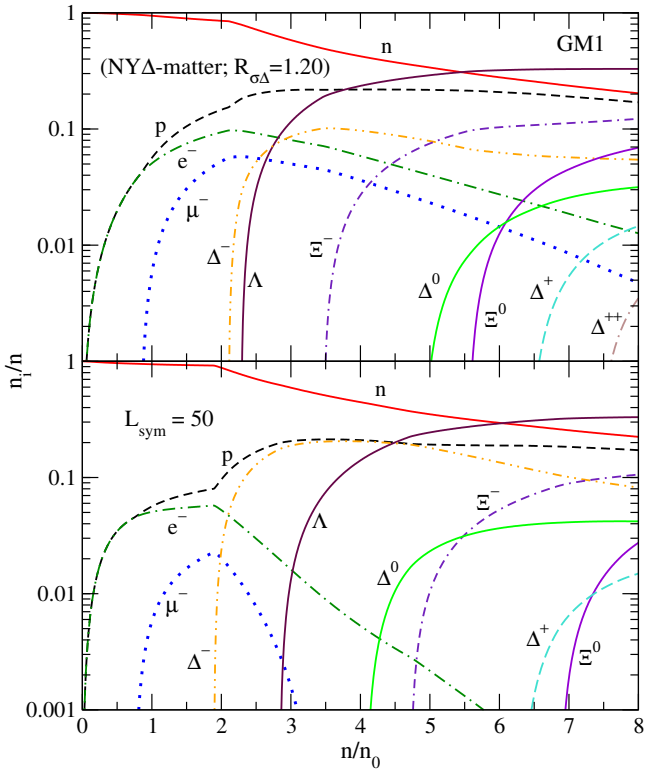

Figure 6.5: Particle populations, n_i (in units of n) as a function of baryon number density for NYΔ-matter ($R_{\sigma\Delta} = 1.20$) with upper panel: $L_{\rm sym}(n_0) = 93.86$ MeV (original), lower panel: $L_{\rm sym}(n_0) = 50$ MeV cases within non-linear coupling (GM1) parametrization.

In order to see the effect of varying $L_{\rm sym}$ on hyperons we plot the strangeness fraction as a function of baryon number density in fig.-6.7 which is defined as [Cavagnoli et al., 2011],

$$f_s = \frac{1}{3}\frac{\sum_Y |s_Y| n_Y}{n}, \tag{6.6}$$

where s_Y, n_Y denote the strangeness and number density of Y-th hyperon respectively. It is seen that f_s is sensitive to varying $L_{\rm sym}$ and decreases with lowering of $L_{\rm sym}$ values. This is due to the fact that higher $L_{\rm sym}$ demands more abundance of protons and so in order to satisfy the charge neutrality condition, negatively charged hyperons has to be brought into consideration which in turn increases f_s. The shifting of hyperon threshold densities to higher densities with lower values of $L_{\rm sym}$ (as seen in figs.-6.5 and 6.6) is also evident from fig.-6.7. The similar strangeness fraction for $L_{\rm sym} = 65, 50, 35$ MeV cases at high densities relates with the almost similar values (approaching zero) of $g_{\rho N}(n)$ (refer to fig.-6.2). In both the coupling parametrization cases, similar f_s values at high density regimes relates to the almost vanishing values of ρ-meson coupling. The delaying appearance of hyperons into NS matter with onset of Δ-quartet is also apparently seen in fig.-6.7.

Due to the significant dependence of matter pressure explicitly over energy density in NS matter, it is noteworthy that the EoSs follow the causality condition (i.e. adiabatic speed velocity, v_s to be subluminal) given by $v_s < c$. Fig.-6.8 displays the adiabatic speed of sound as a function of energy density for different matter compositions with variation in $L_{\rm sym}$ values within non-linear scalar and density-dependent RMF models. It is observed that the EoSs

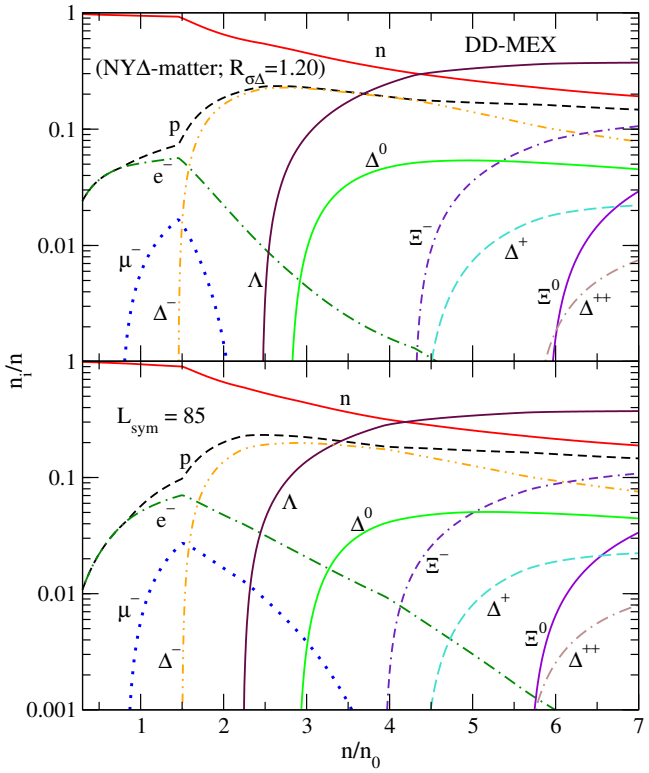

Figure 6.6: Similar to fig.-6.5 but with upper panel: $L_{\rm sym}(n_0) = 49.57$ MeV (original), lower panel: $L_{\rm sym}(n_0) = 85$ MeV cases within density-dependent coupling (DD-MEX) parametrization.

considered in this work satisfy the causality condition which is expected as the EoS model being relativistic in nature. The effect of $L_{\rm sym}$ is more prominent on the lower density regimes. This can be attributed to the diverse $g_{\rho N}$ coupling values at lower densities. Lower values of $L_{\rm sym}$ results in reduced v_s at lower matter densities. Kinks in the lower panels denote onset of heavier baryons in NS matter.

Now we move to examine the effect of $L_{\rm sym}$ on the star properties. The properties of NS for variation of $L_{\rm sym}$ along with matter properties with different EoSs considered in this work have been displayed in tables-6.5, 6.6. $L_{\rm sym}$ has practically no effect on the maximum mass of the star family. However, $L_{\rm sym}$ variation has a commendable impact on the radius of NS configurations. This feature is already clear from the fig.-6.4. We have tabulated the comparative values of radius for typical 1.4 $M_\odot$ mass NS ($R_{1.4}$). With increasing value of $L_{\rm sym}$ the $R_{1.4}$ increases. Consequently, the compactness $C_{1.4}$ decreases. Similar impact is also observed in case of tidal deformability $\Lambda_{1.4}$ with increase of $L_{\rm sym}$ softness decreases. A recent study [Dietrich et al., 2020] based on the joint analysis GW170817 and GW190425 events data reported a radius bound $10.94 \leq R_{1.4}/\text{km} \leq 12.61$ at 90% confidence level. From the EoSs considered in this work, it can be inferred that to satisfy the said $R_{1.4}$ range, the conditions of Δ-resonances onset into NS matter composition and $L_{\rm sym}(n_0) \leqslant 50$ MeV are favourable. Following the $69 \leq L_{\rm sym}(n_0)/\text{MeV} \leq 143$ range deduced from recent PREX-2 data, it is to be noted that DD-MEX parameterization satisfies the $\Lambda_{1.4}$ upper bound (GW170817 event) for $L_{\rm sym}(n_0) \leq 85$ with $R_{\sigma\Delta} = 1.20$.

The variations of compactness parameter and tidal deformability of 1.4 $M_\odot$ NS with

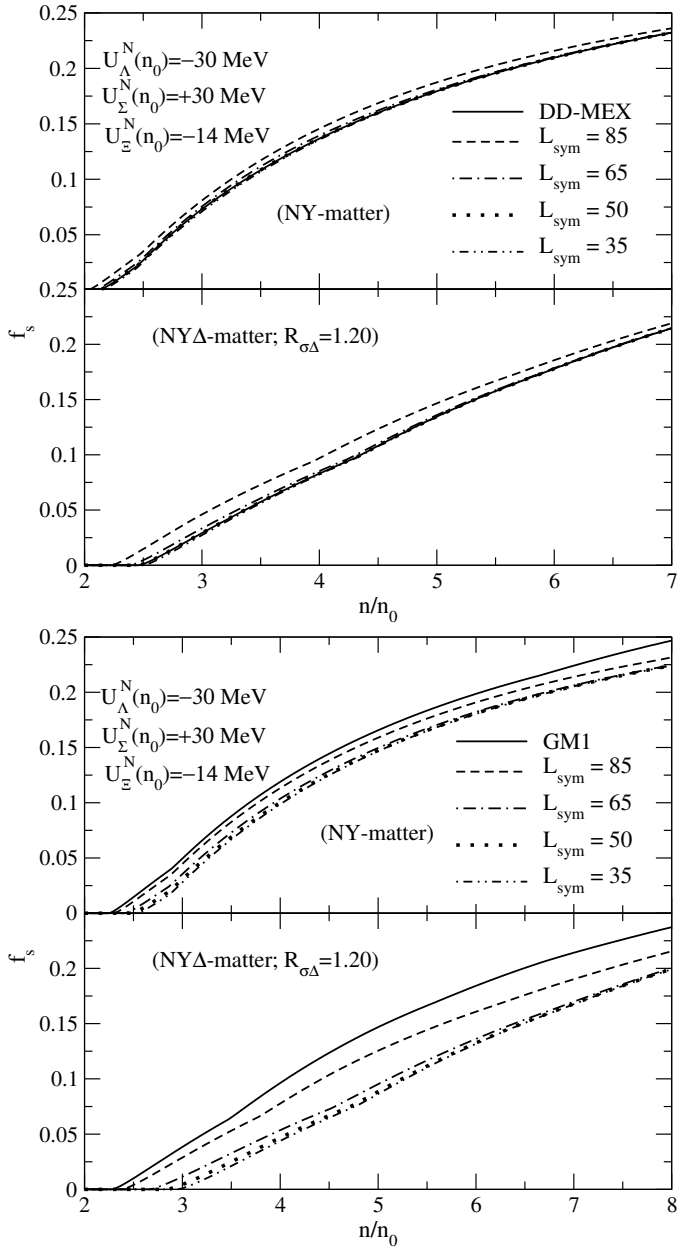

Figure 6.7: Strangeness fraction, f_s as a function of baryon number density for matter composition as, upper panels: NY and lower panels: NYΔ ($R_{\sigma\Delta} = 1.20$) with varying $L_{\rm sym}$ for GM1 and DD-MEX parametrizations. The different curves represent the same cases as captioned in fig.-6.1.

$L_{\rm sym}$ considering various matter compositions are shown in fig.-6.9. The softness decreases in both parametrizations following similar trend of convergence towards higher $L_{\rm sym}$ values. This relates to the fact that lowering of $L_{\rm sym}$ shifts the onset of Δ-quartet to lower density regimes thus increasing compactness and decreasing tidal deformability. The quadratic fit of compactness parameter and tidal deformability as a function of $L_{\rm sym}$ for different matter compositions with GM1 and DD-MEX parametrizations is given by,

$$C_{1.4} \text{ or, } \Lambda_{1.4} = a\ L_{\rm sym}^2 + b\ L_{\rm sym} + c, \tag{6.7}$$

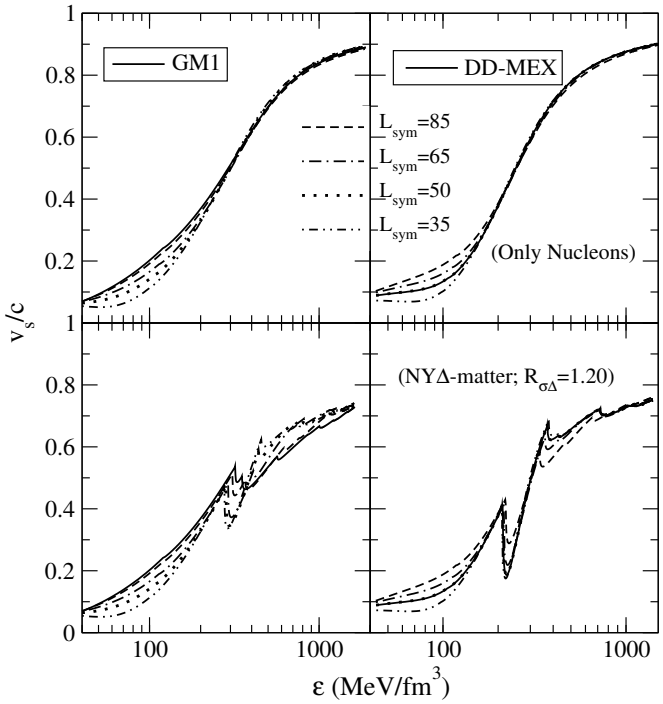

Figure 6.8: Sound velocity (in units of c) as a function of energy density for, upper panels: pure nucleonic, lower panels: Δ-admixed hypernuclear matter ($R_{\sigma\Delta} = 1.20$) with left panels: non-linear (GM1) and right panels: density-dependent (DD-MEX) coupling models. The different curves represent the same cases as captioned in fig.-6.1.

Table 6.7: Coefficient values of the quadratic fits in eqn.-(6.7). The coefficient of determination, $\mathcal{R}^2 \sim 0.999$ for all the fits considered in this work.

	RMF Model	a	b	c
$C_{1.4}$	GM1 (N)	-1.83×10^{-6}	-2.10×10^{-6}	0.1663
	GM1 (NYΔ)	-2.01×10^{-6}	-6.51×10^{-5}	0.1738
	DD-MEX (N)	-1.53×10^{-6}	2.38×10^{-5}	0.1581
	DD-MEX (NYΔ)	-3.31×10^{-6}	0.0002	0.1646
$\Lambda_{1.4}$	GM1 (N)	0.1023	-7.884	719.10
	GM1 (NYΔ)	0.1082	-5.617	458.70
	DD-MEX (N)	0.0623	-3.676	800.80
	DD-MEX (NYΔ)	0.0998	-7.339	622.40

where the coefficient a, b and c values are provided in table-6.7. Similar correlations have been previously discussed in Ref.-Hu et al. [2020] in which linear fit was imposed contrary to the polynomial fit implemented in this work.

Fig.-6.10 shows the variation of dimensionless tidal deformability with NS mass corresponding to different values of density-dependent $L_{\rm sym}$ parameter. As already mentioned, we observe that with higher values of $L_{\rm sym}$, tidal deformability parameter value increases as the matter stiffens. The universal relation between the tidal deformability and mass of NSs has

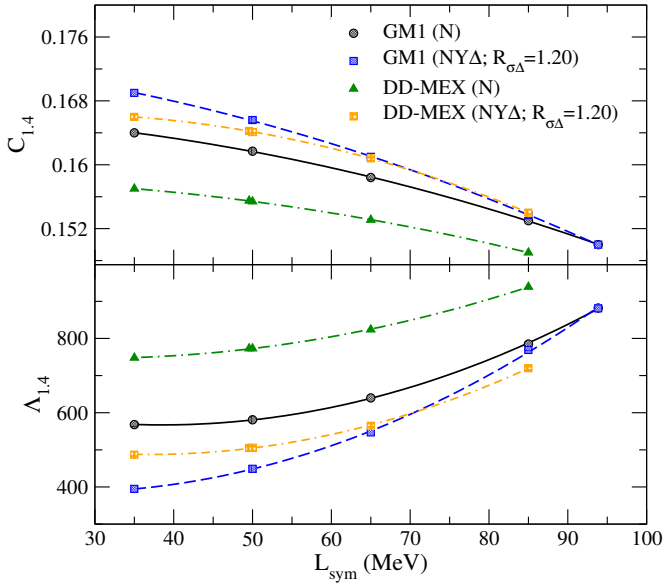

Figure 6.9: Upper panel: Compactness parameter, lower panel: tidal deformability as a function of $L_{\rm sym}$ considering matter composition to be pure N, NYΔ ($R_{\sigma\Delta}$=1.20) with non-linear (GM1) and density-dependent (DD-MEX) coupling models. The different curves denote the EoS models as labelled.

been also discussed in Ref.-Maselli et al. [2013]. The effects of $L_{\rm sym}$ is significant only in case of lower mass stars and for massive stars, these effects are inconsequential. In addition, the inclusion of heavier non-strange baryons softens the EoS at lower density regimes consequently decreasing Λ or, assembling NS matter to be more compact. This relates with the results from refs.-Li and Sedrakian [2019]; Raduta [2021].

6.6 Summary

To summarize, in this chapter, we discuss the density-dependent symmetry energy effects on dense matter EoSs with different matter compositions viz. pure nucleonic, hypernuclear, Δ-admixed hypernuclear within RMF theory framework considering different values of symmetry energy slope $L_{\rm sym}$ to introduce variation of symmetry energy with density. The $L_{\rm sym}$ at saturation is taken to be within the range of $35-85$ MeV. The NS configurations evaluated from the EoSs considered in this work within this range of $L_{\rm sym}$ satisfy the recent astrophysical observable constraints obtained from NICER (PSR J0030 + 0451, PSR J0740 + 6620) and GW observations.

We find that with smaller values of $L_{\rm sym}$, the EoS is evaluated to be softer around density range of $1-2\ n_0$. This is because of the corresponding lower values of $E_{\rm sym}$ in the said density regimes. This results in smaller radii alongside making matter tidally less deformable for intermediate mass NSs viz. 1.4 $M_\odot$. Although the range of $L_{\rm sym}$ considered in this work is consistent with the astrophysical observations, the lower values of $L_{\rm sym}$ are more favourable for the radius observations from NICER as well as estimate of tidal deformability from GW observations. While at the high density regimes, the EoS is similar for all $L_{\rm sym}$ values. This

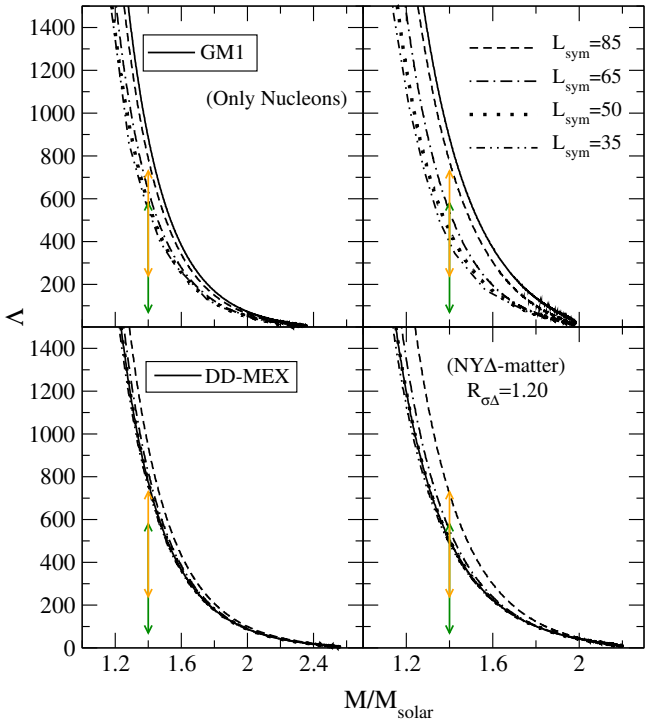

Figure 6.10: Tidal deformability as a function of NS mass for, left panels: pure nucleonic, right panels: NYΔ ($R_{\sigma\Delta} = 1.20$) matter with varying $L_{\rm sym}$ values in upper panels: GM1, lower panels: DD-MEX parametrizations. The different curves represent the same cases as captioned in fig.-6.1. The vertical lines denote the bounds on $\Lambda_{1.4}$ deduced in refs.-Abbott et al. [2019]; Jiang et al. [2020].

attributes to the vanishing ρ meson fields due to small (approaching zero) $g_{\rho N}$ coupling values.

Different values of $L_{\rm sym}$ has also substantial effect on appearance of exotic component of matter. The lower values of $L_{\rm sym}$ shift the threshold density for appearance of hyperons to higher side and favours early appearance of Δ-quartet particles. The early appearance of Δ particles is also one of the causes for higher threshold density for appearance of hyperons with lower values of $L_{\rm sym}$. The early appearance of Δ particles for lower values of $L_{\rm sym}$ makes the EoS softer at lower density regime attributing to smaller radius for stars having mass $\sim 1.4\ M_\odot$. Consequently, the compactness of the stars increases and the deformability decreases with the decreasing values of $L_{\rm sym}$. The different values of $L_{\rm sym}$ do not affect practically the maximum mass of the NS family as at higher density regime, the effect of different values of $L_{\rm sym}$ on the EoS is negligible. This relates with the results from refs.-Cavagnoli et al. [2011]; Providência and Rabhi [2013]. As for higher values of $L_{\rm sym}$, the EoSs do not differ much, the values of compactness and tidal deformability merge at higher values of $L_{\rm sym}$. Hence the possibility of exotic matter appearance with lower values of $L_{\rm sym}$ is most favourable from all astrophysical observations.

However the recent update from nuclear physics sector (PREX-2) suggests higher values of $L_{\rm sym}(n_0)$, which generate tension with the astrophysical observables viz. tidal deformability and radius of a canonical 1.4 $M_\odot$ NS. Considering the viability of inclusion of non-strange Δ-baryons into NS dense matter EoS is seen to be a reasonable option. Moreover, different choices

of coupling models or, parametrizations do not provide a feasible solution to this tension and so should be recalibrated.